Hindawi
International Transactions on Electrical Energy Systems
Volume 2022, Article ID 1348667, 15 pages
https://doi.org/10.1155/2022/1348667

Research Article

A Consensus-Based Distributed Two-Layer Control Strategy with Predictive Compensation for Islanded Microgrid CPS against DoS Attack

Xinrui Liu,[1] **Min Hou**,[1] **Jianjun Yang**,[2] **and Yufei Sun**[1]

[1]*College of Information Science and Engineering, Northeastern University, Shenyang, China*
[2]*State Grid Anhui Electric Power Company, Ma'anshan Power Supply Company, Ma'anshan, China*

Correspondence should be addressed to Xinrui Liu; liuxinrui@ise.neu.edu.cn

Received 20 December 2021; Accepted 20 July 2022; Published 8 September 2022

Academic Editor: Akshay Kumar Saha

Summary. Aiming at the problems of insufficient scalability and slow response speed of the traditional three-layer control structure based on the time scale, this study proposes a distributed two-layer control structure. The primary control uses traditional power-frequency droop control, and the second-level control adopts a consensus protocol to simultaneously achieve the goals of frequency synchronization, frequency non-difference, and power optimization in a distributed manner, which can effectively improve the performance of microgrid frequency adjustment and power optimization. The cyber layer of the AC microgrid cyber-physical system (CPS) is extremely vulnerable to denial-of-service (DoS) attacks, resulting in the inability to achieve control objectives. For this reason, this paper designs a consensus algorithm based on event-triggered and a predictive compensation control link that combines empirical mode decomposition (EMD) and extreme learning machine (ELM) on the basis of the two-layer control structure. Finally, a 4-node islanded microgrid simulation example is used to verify the effectiveness of the proposed strategy. The simulation results show that the two-layer control strategy can achieve microgrid frequency recovery and power optimization while effectively responding to different degrees of DoS attacks.

1. Introduction

The microgrid is one of the most important ways to connect distributed energy to the grid, and it usually works in two modes: islanded and grid-connected mode. In view of the complexity of the microgrid structure and the diversity of control objectives, hierarchical control is usually used to achieve stable and optimized operation of the microgrid. At present, the most widely used is the three-layer control structure based on time scale. [1, 2] Among them, the first level of control directly acts on distributed generators (DGs), its action time is at the level of seconds. The second layer is the secondary adjustment layer, which focuses on the dynamic operation control of the microgrid, its action time has risen from the second level to the minute level. The third layer is the optimization management layer, which has the longest role time and is mainly used to realize power flow control and optimal scheduling. However, due to the long control time and slow response speed of the third layer, before the arrival of the third layer control command, the actual operation of the system may deviate from the expected optimal state due to the inevitable power disturbance in the microgrid, resulting in the reduction of the execution efficiency of power optimization and the deterioration of the economy of the microgrid. [3] Therefore, if the control structure is reduced to two layers, it will improve the operation efficiency of the microgrid.

The flexibility, reliability, and scalability of the distributed control mode are stronger than those of the centralized control mode. Therefore, the distributed control mode [4, 5] is generally used in microgrid. In particular, the multi-agent control method [6, 7] based on the consensus protocol is widely used to solve the problems of voltage regulation, frequency regulation, and optimization [8–11] in

hierarchical control due to its simple structure, flexible control, and only sparse communication. With the continuous development of the intelligent construction of the power grid, the microgrid gradually has the relevant characteristics of the cyber-physical system (CPS). [6, 12] The information layer in the microgrid CPS structure usually involves more control decisions and communication processes, and the use of communication data inevitably leads to communication problems such as delays, packet loss, and communication failures [13, 14]. The traditional three-layer control structure can no longer meet the security requirements of the equipment, and the network security of the microgrid CPS is worth further exploration.

In References [15, 16], a smart energy dispatching method based on distributed economic cooperative predictive control is proposed. In References [17–19], a pilot distributed follower decentralized control strategy for islanded microgrids is proposed, which realizes economic dispatch while ensuring voltage quality and frequency synchronization. However, the above literature are only based on the structure of the physical layer and do not consider the security of the information layer, which is extremely vulnerable to malicious attacks on the network. [20–22] References [6, 12] construct an information-physical collaborative hierarchical control structure and solves random communication problems by designing corresponding observers, controllers, and predictive compensators. In References [23, 24], aiming at the insufficient tolerance of MG to DoS attacks when edge routers in microgrid suffer from DoS attacks, a consensus-based secondary frequency controller with dynamic P-f droop control is proposed and its stability is analyzed. References [25, 26] study the realization of cyber-physical system security and stability control issues in complex networks under non-periodic DoS attacks. However, the above-mentioned literature only studies the network attack on the secondary control level, but does not propose an effective solution to the network attack for a microgrid with third control targets. A fully distributed microgrid frequency recovery and power optimization structure capable of responding to network attacks have not yet appeared. Therefore this paper proposes a distributed two-layer control structure that combines droop control and consensus algorithm in order to improve the performance of microgrid frequency adjustment and power optimization under the consideration of the network being attacked by DoS. The main contributions are as follows:

(1) The distributed control structure designed in this study can overcome the shortcomings of centralized control and transfer the power optimization control to the second layer. While the frequency is restored to the nominal value, the incremental cost(IC) can be consistent, which can effectively improve the optimization operation efficiency of the microgrid.

(2) Aiming at the DoS attacks that occur on the communication link of the cyber layer, the improved consensus algorithm based on event-triggered and predictive compensation that combines EMD and ELM can effectively respond to different degrees of DoS attacks.

2. Microgrid System Modeling

2.1. Multi-Agents Distributed Model. For a MG containing n DGs, DGs are regarded as nodes in the agent communication network, and the communication topology can be represented by an undirected graph G. In graph G, the adjacency matrix $A = (a_{ij})_{n\times n}$ is usually used to describe the relationship between nodes, wherea_{ij} represents the connection weight between node i and node j, and n is the number of nodes. If the j-th node has an edge pointing to the i-th node, then$a_{ij} > 0$, $i \neq j$, otherwise $a_{ij} = 0$, the diagonal element $a_{ii} = 0$.

For a distributed multi-agents control system with n agents, due to the use of distributed control laws, the change of each agent's state depends on its own current state and the current state of its neighboring agents, which can be expressed for

$$u_i(t) = -\sum_{j\in N_i} a_{ij}\big(x_i(t) - x_j(t)\big). \tag{1}$$

Written in matrix form as

$$\begin{cases} \dot{\mathbf{X}} = \mathbf{U} \\ \mathbf{U} = -\mathbf{L}\mathbf{X}. \end{cases} \tag{2}$$

Lemma 1. *Assuming that the multi-agents systems are undirected and connected, then its corresponding Laplacian matrix must be a real symmetric matrix, the aforementioned protocol can achieve the average consistency of the system, namely [23],*

$$x_{1\infty} = x_{2\infty} = \cdots = x_{n\infty} \approx \sum_{i=1}^{n} \frac{x_{i0}}{n}. \tag{3}$$

2.2. Cost Function Model. The operating cost of the i-th DGs can be described as follows:

$$C_i(P_i) = a_i P_i^2 + b_i P_i + c_i \quad i = 1, \ldots, n. \tag{4}$$

The goal of economic dispatch of the islanded microgrid is to minimize the operating cost, namely,

$$C_{\text{total}} = \min \sum_{i=1}^{n} C_i(P_i). \tag{5}$$

The generated power of each distributed power source must meet the power balance constraint conditions:

$$\sum_{i=1}^{n} P_i = \sum_{j=1}^{l} P_{Dj} = P_D. \tag{6}$$

The DG generation power should also meet the following constraints:

$$P_{i,\min} \le P_i \le P_{i,\max} \quad i = 1, \ldots, n. \tag{7}$$

Based on the Lagrangian multiplier method and the equal incremental rate theory, the target formula of

economic dispatch is transformed into an incremental factor synchronization control target, which includes

$$\begin{cases} \lambda_i(P_i) = \dot{C}_i(P_i) = 2a_iP_i + b_i = \lambda^*, & P_{i,\min} < P_i < P_{i,\max} \\ \lambda_i(P_i) = \dot{C}_i(P_i) = 2a_iP_{i\min} + b_i, P_i = P_{i,\min} \\ \lambda_i(P_i) = \dot{C}_i(P_i) = 2a_iP_{i,\max} + b_i, P_i = P_{i,\max} \end{cases}. \tag{8}$$

Eq.(8) explains that if P_i is within the allowable output range, when the IC of all DG is equal to the optimal IC, the total power generation cost of the system is minimum. When P_i reaches the upper or lower limit of capacity, DGi should run on its bounded value, and the rest of the DGs should continue to run according to the above economic dispatch rules. The optimal IC can be calculated as:

$$\lambda^* = \frac{P_D + \sum_{i=1}^{n}(b_i/2a_i)}{\sum_{i=1}^{n}(1/2a_i)}. \tag{9}$$

3. Two-Level Distributed Control Strategy

3.1. Control Structure and Control Objectives. On the basis of P-f droop control, a consistent control strategy based on droop control is proposed to solve the problem of fully distributed data collection. Because there is no leader DG, dependence on the central controller under the centralized control structure is avoided. In this paper, a two-way communication network is adopted. Regarding each DG as an agent, the local controller of each agent exchanges IC information with the local controllers of its neighboring agents. Based on the transmission of IC information, the proposed consistency control strategy can simultaneously achieve frequency adjustment and optimal economic operation.

The hierarchical control structure constructed in this article is different from the traditional three-layer structure. This article only needs to establish a two-layer structure. At the second layer, both power optimization and frequency recovery are realized, aiming to greatly shorten the optimization operation time, and significantly improve the stability and optimization operation efficiency of the microgrid. Taking the i-th DG as an example, the hierarchical control architecture with CPS characteristics is shown in Figure 1.

The control objectives of this microgrid system can be summarized as follows:

Goal 1: Frequency synchronization.

$$\lim_{t\longrightarrow\infty}\left(f_i - f_j\right) = 0, \quad \forall i, j \in \Omega. \tag{10}$$

Goal 2: Frequency error-free.

$$\lim_{t\longrightarrow\infty}\left(f_i - f_{MG}^{\text{ref}}\right) = 0, \quad \forall i \in \Omega. \tag{11}$$

Goal 3: Consistent incremental cost.

$$\lim_{t\longrightarrow\infty}\left(\lambda_i(P_i) - \lambda_j\left(P_j\right)\right) = 0, \quad \forall i, j \in \Omega. \tag{12}$$

In addition, the system also needs to meet the power balance constraints and the upper and lower limits of DG generation power, which have been explained in the previous section and will not be explained here.

3.2. Primary Control Strategy. The primary control considers the use of traditional droop control to achieve frequency stability, which is given as follows:

$$f_i = f_{MG}^{\text{ref}} - m_i\left(P_i - P_i^{\text{ref}}\right). \tag{13}$$

For a microgrid composed of multiple DGs in parallel, the frequency of each DG is equal, that is, f_i is equal. However, droop control is a differential control. Therefore, to make the frequency of each DG equal to the system frequency, a common method is to add frequency compensation to restore f_i to f_{MG}^{ref}.

3.3. Secondary Frequency Modulation and Power Optimization Control Strategy. The primary control only acts on the controllable DG unit of the physical layer, and the second layer control has been upgraded from the physical layer to the cyber layer, and requires sparse communication between DGs to achieve information exchange and coordinated control. Since the control scheme adopts a ring communication network to transmit the IC information of DGs, it can eliminate the requirement of Leader DG, reduce the information exchange between DGs, and improve efficiency. Since reactive power does not incur any costs, there is no need to discuss reactive power sharing schemes.

For the goal of frequency error-free control, it is realized by adding a PI controller, and the compensation amount is calculated according to the following formula:

$$\delta f = k_{P,i}\left(f_{MG}^{\text{ref}} - f_i\right) + k_{I,i}\int\left(f_{MG}^{\text{ref}} - f_i\right)\mathrm{d}t. \tag{14}$$

Aiming at the realization of the power optimization goal, without considering the DG capacity constraints, the control equation is designed as follows [21]:

$$P_i^{\text{ref}} = \frac{\left(\sum_{j=1}^{n} a_{ij}\lambda_j - \lambda_i - b_i\right)}{2a_i}, \tag{15}$$

$$\begin{aligned} f_i = {} & f_{MG}^{\text{ref}} - m_i\left(P_i - P_i^{\text{ref}}\right) + k_{P,i}\left(f_{MG}^{\text{ref}} - f_i\right) \\ & + k_{I,i}\int\left(f_{MG}^{\text{ref}} - f_i\right)\mathrm{d}t. \end{aligned} \tag{16}$$

The IC information is selected as the consistency variable, and the local controller of DGi updates the reference power P_i^{ref} according to (15). In addition, the system frequency is stabilized based on (16). That is to say, the proposed method can update the output power reference value according to the neighboring IC information, and realize economic operation and frequency recovery, which is convenient to implement and simplifies the control loop.

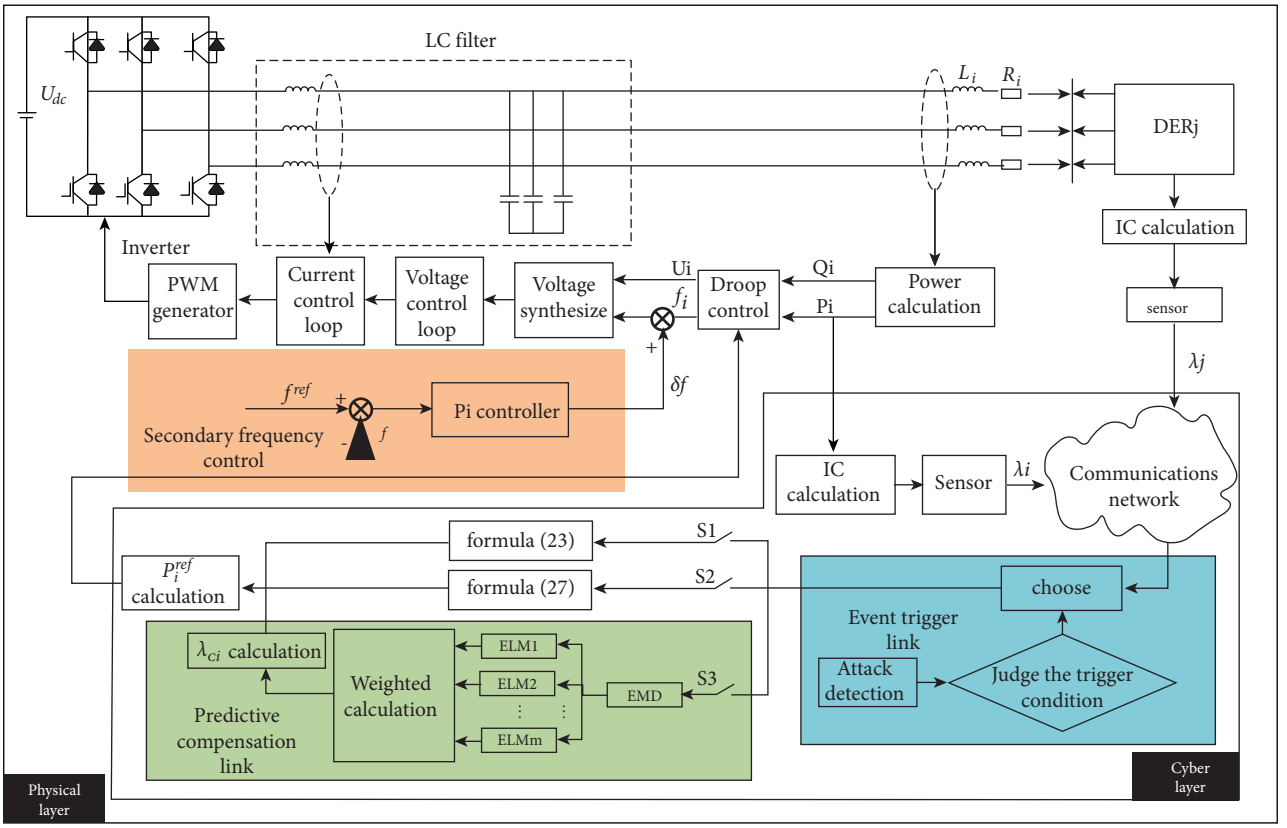

Figure 1: The hierarchical control architecture diagram of the i-th DG.

The process of equations (15) and (16) to achieve frequency recovery and power optimization is as follows.

The matrix form of (15) and (16) is expressed as follows:

$$\mathbf{P}^{\text{ref}} = \frac{1}{2}\mathbf{a}^{-1}(\mathbf{A}\boldsymbol{\lambda} - \boldsymbol{\lambda} - b), \tag{17}$$

$$\mathbf{f} = f_{MG}^{\text{ref}} - \mathbf{M}\left(P - \mathbf{P}^{\text{ref}}\right) + \mathbf{K}_p\left(f_{MG}^{\text{ref}} - \mathbf{f}\right) + K_I\Delta, \tag{18}$$

where $\mathbf{P}^{\text{ref}} = [P_1^{\text{ref}}, P_2^{\text{ref}}, \ldots, P_n^{\text{ref}}]^T\mathbf{a} = \text{diag}(a_1, a_2, a_3, \cdots a_n$ $\boldsymbol{\lambda} = [\lambda_1, \lambda_2, \cdots, \lambda_n]^{\text{T}}\mathbf{b} = [b_1, b_2, \ldots, b_n]^T\mathbf{K}_p = \text{diag}(k_{p,1}, k_{p,2}, \ldots, k_{p,n})\mathbf{K}_I = \text{diag}(k_{I,1}, k_{I,2}, \ldots, nk_{I,n})\mathbf{f} = [f_1, f_2, \ldots, f_n]^T$, $\mathbf{f}_{MG}^{\text{ref}} = \text{f}_{MG}^{\text{ref}}\mathbf{1}^n$, $\mathbf{P} = [P_1, P_2, \ldots, P_n]^T$, $\Delta = \int(\mathbf{f}_{MG}^{\text{ref}} - \mathbf{f})\text{d}t$.

The design of the adjacency matrix in this paper is as follows:

$$\mathbf{A} = \begin{bmatrix} 0 & 1 & \cdots & 0 & 1 \\ 1 & 0 & 1 & \cdots & 0 \\ 0 & 1 & 0 & \cdots & 0 \\ \cdots & \cdots & \cdots & \cdots & 1 \\ 1 & 0 & \cdots & 1 & \cdots \end{bmatrix}_{n\times n}. \tag{19}$$

According to (17) and (18), (20) can be obtained as follows:

$$\mathbf{L}\boldsymbol{\lambda} = 2\mathbf{a}\mathbf{M}^{-1}\left[(\mathbf{E} + \mathbf{K}_P)\Delta\mathbf{f} + \mathbf{K}_I\Delta\right], \tag{20}$$

where $\boldsymbol{\Delta}\mathbf{f} = \mathbf{f}_{MG}^{\text{ref}} - \mathbf{f}$.

The Laplacian matrix of the communication graph has the following form:

$$\mathbf{L} = \begin{bmatrix} 2 & -1 & \cdots & 0 & -1 \\ -1 & 2 & -1 & \cdots & 0 \\ 0 & -1 & 2 & \cdots & 0 \\ \cdots & \cdots & \cdots & \cdots & -1 \\ -1 & 0 & \cdots & -1 & 2 \end{bmatrix}_{n\times n}. \tag{21}$$

According to (20), (22) can be obtained as follows:

$$-\sum_{j=1}^{n} a_{ij}\left(\lambda_i - \lambda_j\right) = \kappa_i\Delta f_i + \zeta_i\int\Delta f_i\text{d}t, \tag{22}$$

where $\Delta f_i = f_{MG}^{\text{ref}} - f_i$, $\kappa_i = (-2a_i/m_i)(1 + k_{p,i})$, and $\zeta_i = -2a_ik_{I,i}/m_i$.

The left side of (22) denotes the consistency control, which can be defined as follows:

$$u_i(t) = -\sum_{j=1}^{n} a_{ij}\left(\lambda_i - \lambda_j\right). \tag{23}$$

Taking the IC as a consistency variable, the state of each variable will eventually be consistent under the control of the consistency algorithm, that is: $\lambda_i = \lambda_j$. Thus,

$$\kappa_i\Delta f_i + \zeta_i\int\Delta f_i\text{d}t = 0. \tag{24}$$

From the expressions of κ_i andζ_i, we can see that both κ_i andζ_i are negative constants. Therefore, if (24) holds,$\Delta f_i = 0$. So under the consensus algorithm and PI controller-based secondary frequency control, the frequency error will be eliminated. That is, when $t \longrightarrow \infty$, $\Delta f_i \longrightarrow 0$. According to (22), it can be concluded that when the IC of each DG is equal, there is $f_{MG}^{\text{ref}} - f_i = 0$, that is, the frequency recovery of DGi is realized. It is concluded that the proposed control scheme can achieve power optimization and secondary frequency control on the same time scale. Compared with the three-layer control structure, it can effectively shorten the operating time of the system and improve the operating efficiency of the microgrid.

4. Control Strategies to against DOS Attacks

4.1. DoS Attack Modeling. The communication between DGs in MG is implemented based on the UDP protocol, which is a universal and easily affected protocol. In the process of communication, the data packets containing the IC information are transmitted through the channel, received by the data receiver of the DGs, written into the data buffer, and processed by the consistency controller in the DGs. Due to the openness of the communication network, the secondary control layer is easily attacked by attackers. The data path from the cyber layer DGi to DGj is shown in Figure 2.

The goal of DoS attack is to try to destroy the availability of data transmission and block the information transmission between DGs, thus making the secondary control strategy of microgrid invalid. Due to the attacker's limited energy, DoS attacks are distributed in sequence in time. Define the attack start time on the communication link.

$\{i, j\} \in \Omega$ asT_k^{ij}, $T_k^{ij} \geq 0$.The duration of the attack is $\tau_k^{ij} \tau_k^{ij} \geq 0 k \in N^+$, and satisfied $T_{k+1}^{ij} > T_k^{ij} + \tau_k^{ij}$. Then the k-th DoS attack can be expressed as $\mathbf{U}_k^{ij} = [T_k^{ij}, T_k^{ij} + \tau_k^{ij}]$. $\mathbf{U}_{(t_0,t)}^{ij} = \bigcup \mathbf{U}_k^{ij}[t_0, t]$ represents the total DoS attack sequence set in the time interval $[t_0, t]$.

Assuming that data packets are transmitted through channels, routers provided by service providers, and other network equipment. Due to the openness and sharing of wireless media, sensor nodes are vulnerable to different network attacks. In this paper, it is assumed that the attacker launches DoS attacks on the router of the service provider, and the most direct impact of DoS attacks is the loss of data packets.

Define α_i andα_j as the packet loss rate of transmitted data after DGi and DGj are attacked respectively. The Equation is as follows:

$$u_i(t) = -\sum_{j=1}^{n} a_{ij}\left[(1-\alpha_i)\lambda_i - \left(1-\alpha_j\right)\lambda_j\right]. \tag{25}$$

When a DG in the microgrid suffers DoS attacks, the impact of the attack will gradually propagate throughout the network, which will seriously affect the authenticity of the data. Since DG can only judge the existence of attacks by λ_i, λ_j and the tracking error. However, the tracking error will also converge to 0 in the presence of DoS attacks. Therefore, the DG itself can not directly use the above information to judge whether there is an attack or not, nor can it eliminate the influence of attacks.

4.2. DoS Attack Detection. Intrusion detection, as an important means to ensure network security, can monitor network activities in real-time, judge the state of equipment, find the attacked equipment in time, and then take corresponding countermeasures. Traditional intrusion detection methods are to identify behaviors that are significantly different from normal traffic as abnormal behaviors. This method does not require prior knowledge of abnormal network behaviors and can achieve better detection accuracy.

Under the CPS architecture, it is known that the attack will cause the data packets sent by the router to be abnormal, so the change of the data packets can be used as the basis for detection.

Define the detection function for DoS attacks on communication link $\{i, j\} \in \Omega$ as$\theta_{ij}(t)$, $\theta_{ij}(t) \in \{0, 1\}$. When DoS attacks occur on the communication link $\{i, j\} \in \Omega$, the detection function $\theta_{ij}(t)$ can detect that the attack has occurred, and its value is set to 1 and kept, denoted as$\theta_{ij}(t) : \longrightarrow 1$. When there are no DoS attacks, the value of $\theta_{ij}(t)$ is set to 0 and kept, which is recorded as$\theta_{ij}(t) : \longrightarrow 0$. All $\theta_{ij}(t)$ are independent. The mathematical probability formula combined with the previous DoS attack model can be expressed as follows:

$$\begin{cases} \text{Prob}\left\{\theta_{ij}(t) = 1\right\} = E\left\{\theta_{ij}(t)\right\} = \gamma_{ij} \\ \text{Prob}\left\{\theta_{ij}(t) = 0\right\} = 1 - E\left\{\theta_{ij}(t)\right\} = 1 - \gamma_{ij} \end{cases}, \tag{26}$$

where $\gamma_{ij} \in [0, 1]$ is a known constant and is related toα_i andα_j.

4.3. Event-Triggered Control. Taking into account the limited communication bandwidth between the agents in the microgrid, this paper uses event-triggered control to reduce the amount of communication between the agents. Due to the different degrees of DoS attacks, the defined packet loss rate α is a constant between $[0, 1]$. When the packet loss rate is within the controllable range, an improved consistency formula based on event-triggered is proposed, and the influence of DoS attacks on the consistency control process is overcome by setting the gain coefficient $k_{\lambda i}$ and the correction amountζ. However, when the packet loss rate is too high, that is, the extreme case of DoS attacks, the above methods can no longer meet the control requirements of the system. Therefore, it is considered to replace the real data with the data obtained by prediction compensation to complete the IC consistency control process.

The improved consistency formula based on event-triggered is as follows:

$$u_i(t) = -k_{\lambda i}\sum_{j=1}^{n} a_{ij}\left[(1-\alpha_i)\lambda_i - \left(1-\alpha_j\right)\lambda_j\right] + \zeta. \tag{27}$$

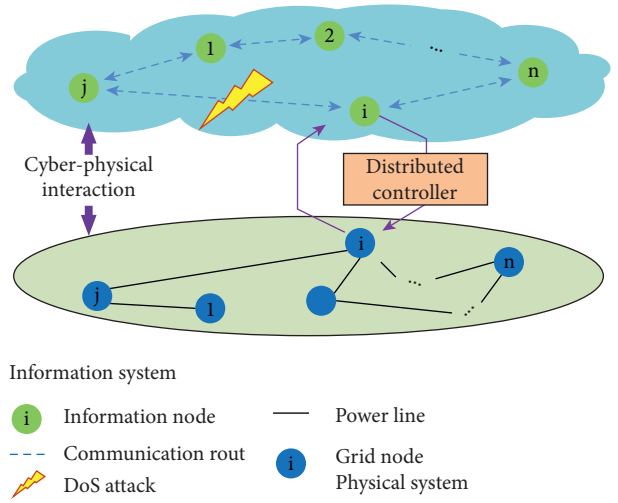

Figure 2: Data path from DGi to DGj.

This paper takes DG1 and DG2 as examples to give a brief proof process to illustrate the conditions that (27) must meet to complete the consistency control process. It is known that the incremental costs λ_1 andλ_2 satisfy the first-order equation.

$$\begin{cases} \dot{\lambda}_1 = u_1 \\ \dot{\lambda}_2 = u_2, \end{cases} \tag{28}$$

where

$$u_1(t) = -k_{\lambda 1}\sum_{j=1}^{n} a_{1j}[(1-\alpha_1)\lambda_1 - (1-\alpha_j)\lambda_j] + \zeta$$
$$u_2(t) = -k_{\lambda 2}\sum_{j=1}^{n} a_{2j}[(1-\alpha_1)\lambda_1 - (1-\alpha_j)\lambda_j] + \zeta$$

Laplace transformation on the above formulas can be obtained:

$$\lambda_1(s) = \frac{k_{\lambda 1}\sum_{j=1}^{n} a_{1j}\left(1-\alpha_j\right)\lambda_j(s) + \lambda_1(t)|_{t=0} + \zeta/s}{s + k_{\lambda 1}\sum_{j=1}^{n} a_{1j}(1-\alpha_1)}, \tag{29}$$

$$\lambda_2(s) = \frac{k_{\lambda 2}\sum_{j=1}^{n} a_{2j}\left(1-\alpha_j\right)\lambda_j(s) + \lambda_2(t)|_{t=0} + \zeta/s}{s + k_{\lambda 2}\sum_{j=1}^{n} a_{2j}(1-\alpha_2)}. \tag{30}$$

In the formulas, $\lambda_1(s)$ and $\lambda_2(s)$ are the state quantities of the IC after Laplace transformation, and $\lambda_1(t)|_{t=0}$ and$\lambda_2(t)|_{t=0}$ are the initial values of the IC of DG1 and DG2, respectively. Define the IC state deviation obtained by DG1 and DG2 as follows:

$$e(t) = \lambda_1(t) - \lambda_2(t), \tag{31}$$

$$\lim_{t\longrightarrow\infty} e(t) = \lim_{s\longrightarrow 0} se(s) = \lim_{s\longrightarrow 0} s\left(\lambda_1(s) - \lambda_2(s)\right) = \frac{\zeta\left[k_{\lambda 2}\sum_{j=1}^{n} a_{2j}(1-\alpha_2) + k_{\lambda 1}\sum_{j=1}^{n} a_{1j}(1-\alpha_1)\right]}{k_{\lambda 1}\sum_{j=1}^{n} a_{1j}(1-\alpha_1)\cdot k_{\lambda 2}\sum_{j=1}^{n} a_{2j}(1-\alpha_2)}. \tag{32}$$

At this time, when $k_{\lambda i}$ andζ meet the following condition, the system can meet the consistency requirements.

$$\frac{\zeta\left[k_{\lambda 2}\sum_{j=1}^{n} a_{2j}(1-\alpha_2) + k_{\lambda 1}\sum_{j=1}^{n} a_{1j}(1-\alpha_1)\right]}{k_{\lambda 1}\sum_{j=1}^{n} a_{1j}(1-\alpha_1)\cdot k_{\lambda 2}\sum_{j=1}^{n} a_{2j}(1-\alpha_2)} = 0. \tag{33}$$

Set the triggered functions to $S_1(t)$, $S_2(t)$ and$S_3(t)$, which are defined as follows according to the previous description:

$$\begin{cases} S_1(t) = \left\{(i,j)\in\Omega:\ \theta_{ij}(t) = 0\right\} \\ S_2(t) = \left\{(i,j)\in\Omega:\ \theta_{ij}(t) = 1 \text{and} \alpha_i \cup \alpha_j \in (0,1)\right\}. \\ S_3(t) = \left\{(i,j)\in\Omega:\ \theta_{ij}(t) = 1 \text{and} \alpha_i \cap \alpha_j = 1\right\} \end{cases} \tag{34}$$

When the triggered condition of (34) is met, DGi will send a request to the DGj to obtain its state information and update the control parameters. Among them, triggered condition $S_1(t)$ means that when the detection function$\theta_{ij}(t) = 0$ on the communication link$\{i,j\}\in\Omega$, that is, when the link is not subjected to DoS attacks, the control process is directly completed by (23). $S_2(t)$ means that when$\theta_{ij}(t) = 1$ on the communication link$\{i,j\}\in\Omega$, that is, when the link is under DoS attacks and the packet loss rate is within the controllable range, the control process is completed by (27). $S_3(t)$ means that when$\theta_{ij}(t) = 1$ on the communication link$\{i,j\}\in\Omega$, that is, when the link is under DoS attacks and the packet loss rate is 1, the control process is completed by the predictive compensation control.

4.4. Predictive Compensation Control. The inability of agent i to receive the data of agent j will result in the inability to achieve the IC consistency, and thus fail to complete the restoration of the system frequency on the same time scale. In order to avoid the coupling problem between agents caused by directly predicting the data of agents, this paper uses the historical power data of agents at a moment in time, and calculates the IC through the predicted power, so as to obtain the corresponding control parameters.

In order to better analyze the consistent dynamic characteristics, Equation (23) is discretized. Let the sampling

period be T_s, $t = t_0 + kT_s$, abbreviated as $t = k$. $\lambda(k)$ is sent every sampling period, and the corresponding discrete consistency algorithm can be written as follows:

$$\lambda_i(k+1) = \sum_{j=1}^{n} w_{ij}(k)\lambda_j(k) = \lambda_i(k) + \sum_{j\neq i} w_{ij}(k)\big(\lambda_j(k) - \lambda_i(k)\big), \quad i = 1, 2, \ldots, n. \tag{35}$$

The corresponding matrix form is

$$\boldsymbol{\lambda}(k+1) = \mathbf{W}(k)\boldsymbol{\lambda}(k). \tag{36}$$

In order to ensure the consistency of the system and still converge to the average value, $\mathbf{W}(k)$ is constructed according to the Metropolis method.

According to whether the agent is attacked by DoS, set the control parameter λ_{Ai} to indicate the latest update signal obtained by the agent i based on the event-triggered. When the triggered condition$S_3(t)$ is met, λ_{Ai} can be expressed as

$$\lambda_{Ai} = \theta_{ij}(k)\lambda_{ci} + \big(1 - \theta_{ij}(k)\big)\lambda_i. \tag{37}$$

Predictive compensation control is designed according to the following steps:

(1) EMD is used to preprocess the historical data, and multiple intrinsic mode functions(IMFs) are obtained from the historical data. The IMF component must meet the following two conditions:

(i) During the entire period, the number of extreme points and zero crossing points are equal, or the difference does not exceed 1

(ii) At any moment, the average value of the upper envelope and the lower envelope is zero

(2) For this series of IMFs, a sliding window is used to intercept historical time series to obtain data samples. Intercept the data sample of length D as an input sample, then the data at the next moment is the expected value output by the ELM model. [12].

EMD is carried out in accordance with the flow chart given in Figure 3. The structure of the entire ELM network is shown in Figure 4.

Suppose that the input layer of the network has n neurons, the output layer has m neurons, and the hidden layer has L neurons. The activation function is $G(\cdot)$. Input sample $\mathbf{X} = [IMF_1, IMF_2, \cdots, IMF_n]^T$, output sample $\mathbf{Y} = [p_{ELM1}, p_{ELM2}, \cdots, p_{ELMm}]^{\mathrm{T}}$. The output function of the ELM model can be expressed as

$$f_{\mathbf{L}}(\mathbf{X}) = \sum_{j=1}^{\mathbf{L}} \beta_j G\big(w_j \cdot IMF_i + h_j\big), \quad i = 1, 2, \cdots, n. \tag{38}$$

Where: $w_j = [w_{j1}, w_{j2}, \cdots w_{jn}]^T$, $\beta_j = [\beta_{j1}, \beta_{j2}, \cdots \beta_{jm}]^{\mathrm{T}}$ are the input and output connection weight of the j-th hidden layer neuron.

(3) In order to make the model with the smallest prediction error have a larger weight, the outputs of m ELMs are weighted as follows. The weighted result is

$$P_{ELM} = \sum_{i=1}^{m} \eta_i P_{ELMi}. \tag{39}$$

Where: $\eta_i = (\sum_{i=1}^{m} |e_i| - |e_i|)/(m-1)\sum_{i=1}^{m} |e_i|$. $e_i = P_i - P_{ELMi}$.

Then when the agent is attacked, the IC obtained after the predictive compensation control is as follows:

$$\lambda_{ci} = 2a_i P_{ELM} + b_i. \tag{40}$$

5. Calculation Examples and Simulation

5.1. Simulation Model. In this section, the simulation topology is a four-node microgrid system, as shown in Figure 5.

The MATLAB/SIMULINK to verify the two-layer control strategy proposed above. The microgrid system consists of 4 DGs, the impedance of the power supply is taken as $Z_i = 0.0679 + j4.11 \times 10^{-4}\Omega$. The line impedances meet $Z_{l1} = Z_{l3}$ and$Z_{l2} = Z_{l4}$. Taking as $0.175 + j4.04 \times 10^{-4}\Omega$ and$0.12 + j4.04 \times 10^{-4}\Omega$. The simulation parameters and cost coefficients of each DG are shown in Table 1.

5.2. Performance Test and Comparison under Two-Layer Control Structure

5.2.1. Comparison with Traditional Three-Layer Control. In order to verify the advanced nature of the proposed control strategy, the two-layer control method in this study is compared with the distributed three-layer control method designed in Reference [27]. Set the simulation environment as: $0 \sim 1s$, only droop control is used, and at $t = 1s$, the upper control is activated. The simulation results under the two control strategies are shown in Figure 6.

Figures 6(a)–6(c) are the simulation results of the traditional three-layer control method, and Figures 6(d)–6(f) are the simulation results of the two-layer control method proposed in this paper. It can be seen that after the upper-layer control is activated, both methods can achieve the goals of frequency regulation and power optimization, but compared with the three-layer control method corresponding to Figures 6(a)–6(c), the method proposed in this paper has a faster power optimization speed. The traditional three-layer control needs 0.5 s to achieve incremental factor synchronization, while the control proposed in this paper only needs 0.2 s, which shows that the performance of the two-layer control strategy is better than the traditional three-layer control.

5.2.2. System Performance during Load Fluctuations. This part tests the frequency recovery and power optimization effects when the load fluctuates. The system is connected to the control strategy proposed in this study for power

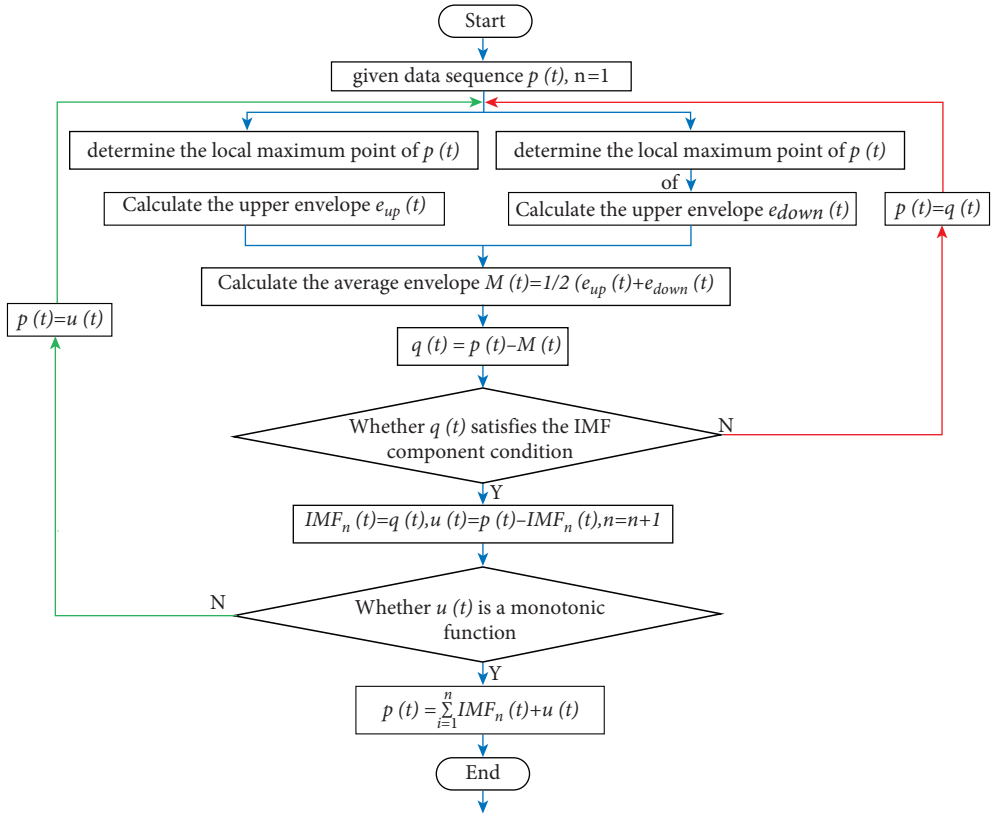

Figure 3: Flow chart of EMD algorithm.

optimization and frequency recovery at $t = 1s$, and disconnected at $t = 6s$.Set the simulation environment as: (1) At $t = 2s$, Load 1 increases to 70 kw. (2) At $t = 3s$, Load 2 increases to 100 kw. (3) At $t = 4s$, Load 3 is reduced to 70 kw. (4) At $t = 5s$, Load 4 is reduced to 60 kw. The simulation results are shown in Figure 7.

Figures 7(a)–7(c) show the changes in the output active power, incremental cost, and frequency of these four DGs, respectively. As can be seen from Figure 7(b), the initial values of ICs are 0.30750.24840.2865, 0.2306. After starting the control strategy at $t = 1s$, the IC of each DG tends to be consistent and finally stabilizes at 0.2651. After the load demand changes, the IC can still be consistent. It can be concluded that no matter how the load is changed, the IC of each DG can be driven to the same level under the control strategy designed in this study, so the control objectives are well met. As can be seen from Figure 7(c), the frequency of the microgrid can be stabilized at the nominal value of 50 Hz, and the frequency changes little. Therefore, the proposed control scheme can effectively realize the economic operation and frequency adjustment of the islanded microgrid without considering the DG capacity constraints.

5.2.3. System Plug and Play Performance. The distributed control method requires the system to be able to meet the change of topology, so in order to verify the plug-and-play performance of the method in this paper, the simulation process is as follows: The islanded microgrid runs under the condition of total constant load demand of 280 kW, the specific load requirements are shown in Table 2. The system accesses the second-layer control strategy for power optimization and frequency recovery at $t = 1s$, and disconnects

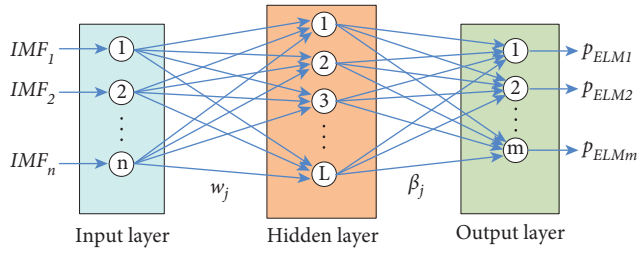

Figure 4: Topology diagram of ELM structure.

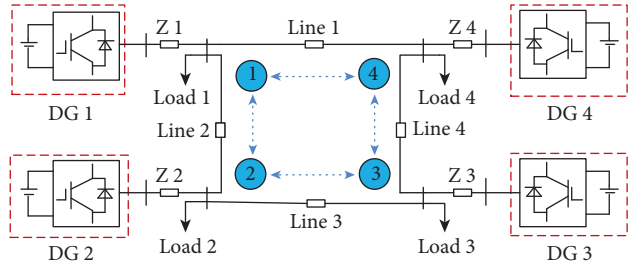

Figure 5: Islanded microgrid structure.

Table 1: Simulation parameters and cost coefficients of each DG.

DGi	P_i^{ref}	m_i	Load1~Load4	a_i	b_i	c_i
DG1	80×10^3	1×10^{-5}	$60kw + 10jk\text{Var}$	1.594×10^{-3}	2.0252×10^{-2}	0.8466
DG2	70×10^3	1×10^{-5}	$90kw + 10jk\text{Var}$	1.195×10^{-3}	5.6606×10^{-2}	0.5146
DG3	60×10^3	1×10^{-5}	$80kw + 0jk\text{Var}$	1.743×10^{-3}	4.1998×10^{-2}	1.2948
DG4	50×10^3	1×10^{-5}	$70kw + 10jk\text{Var}$	1.361×10^{-3}	6.6732×10^{-2}	0.6972

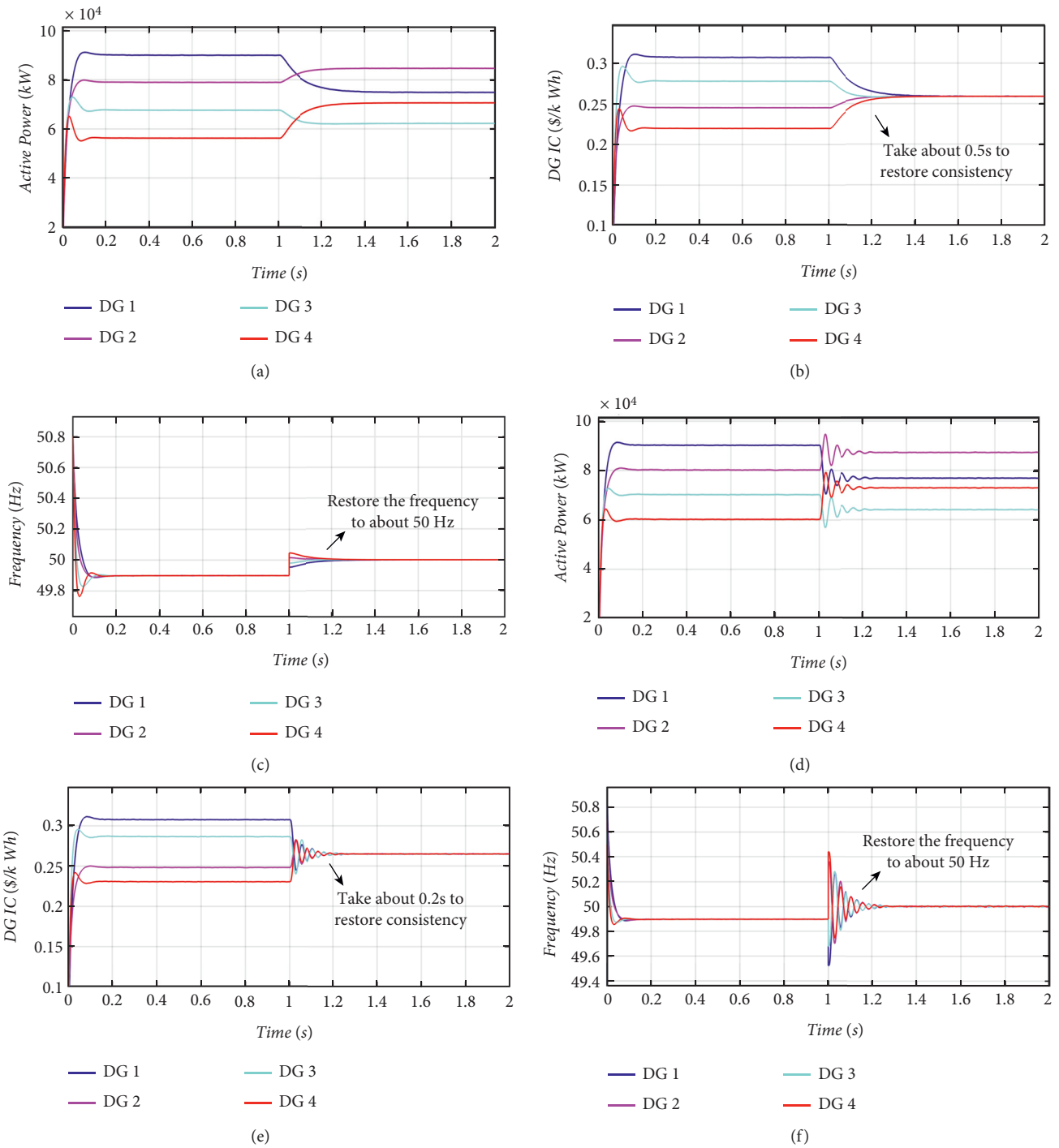

Figure 6: Comparison of control effects of two hierarchical structures.

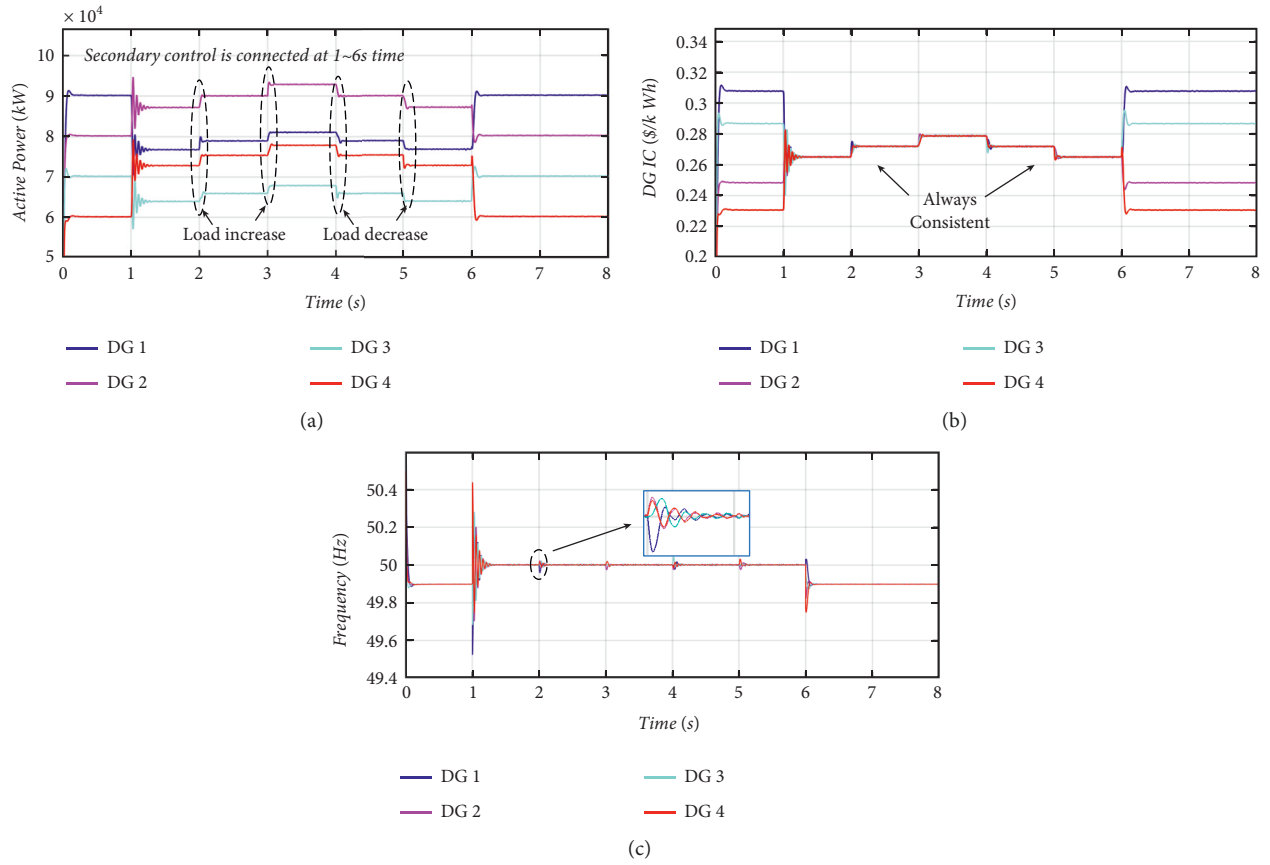

Figure 7: Frequency recovery and power optimization results when load fluctuates.

Table 2: Load demand of each DG.

Loadi	Load1	Load2	Load3	Load4
Value,kW	0	100	90	90

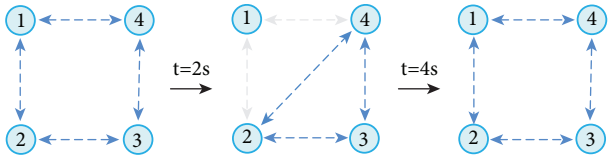

Figure 8: Schematic diagram of communication topology changes.

at $t = 6s$. Set the simulation environment as: (1) At $t = 2s$, DG1 is cut off from system. (2) When $t = 4s$, DG1 is put into the system, and the connection with the system is restored. Figure 8 shows the change in communication topology. The other control parameters and cost coefficients of DG are the same as above and remain unchanged. The simulation results are shown in Figure 9.

As can be seen from Figures 9(a)–9(c), the system can operate stably during the DG input and removal process. Figure 9(a) shows that due to DG1 exiting operation at $t = 2s$, the output power of DG1 is reduced to zero, and DG2, DG3, and DG4 share the total load of the system. At $t = 4s$, DG1 reconnects to the microgrid, and its output power increases from 0 to 7.237 kW. Figure 9(b) shows that in the whole process, although the DGs have changed, the ICs of DGs participating in the power supply are always consistent, so the control requirements can be well met. In addition, Figure 9(c) shows that when the DGs change, the frequency fluctuation can be restored to the nominal value in a short time. Therefore, the proposed control method can well meet the plug-and-play requirement of the microgrid system.

5.2.4. DoS Attack Impact Analysis. As mentioned earlier, the impact of DoS attacks is modeled as data loss that occurs on the communication link $\{i, j\} \in \Omega$, the size of the packet loss rate directly affects the speed and the effect of the consistency convergence process. In order to analyze the impact of different packet loss rates on system control objectives, the simulation process is set as follows: The studied islanded microgrid runs under the simulation parameters of Table 1, and accesses the second-layer control strategy at $t = 4s$, and disconnects at $t = 6s$. In the communication system, the data transmitted by DG1 to other DGs during the period $t_1 = 2s$ to $t_2 = 4s$ is under attack, and the packet loss rate is α_1. The results of the system frequency and the IC of each DG in the period $t_1 \sim t_2$ under different packet loss rates are shown in Figure 10.

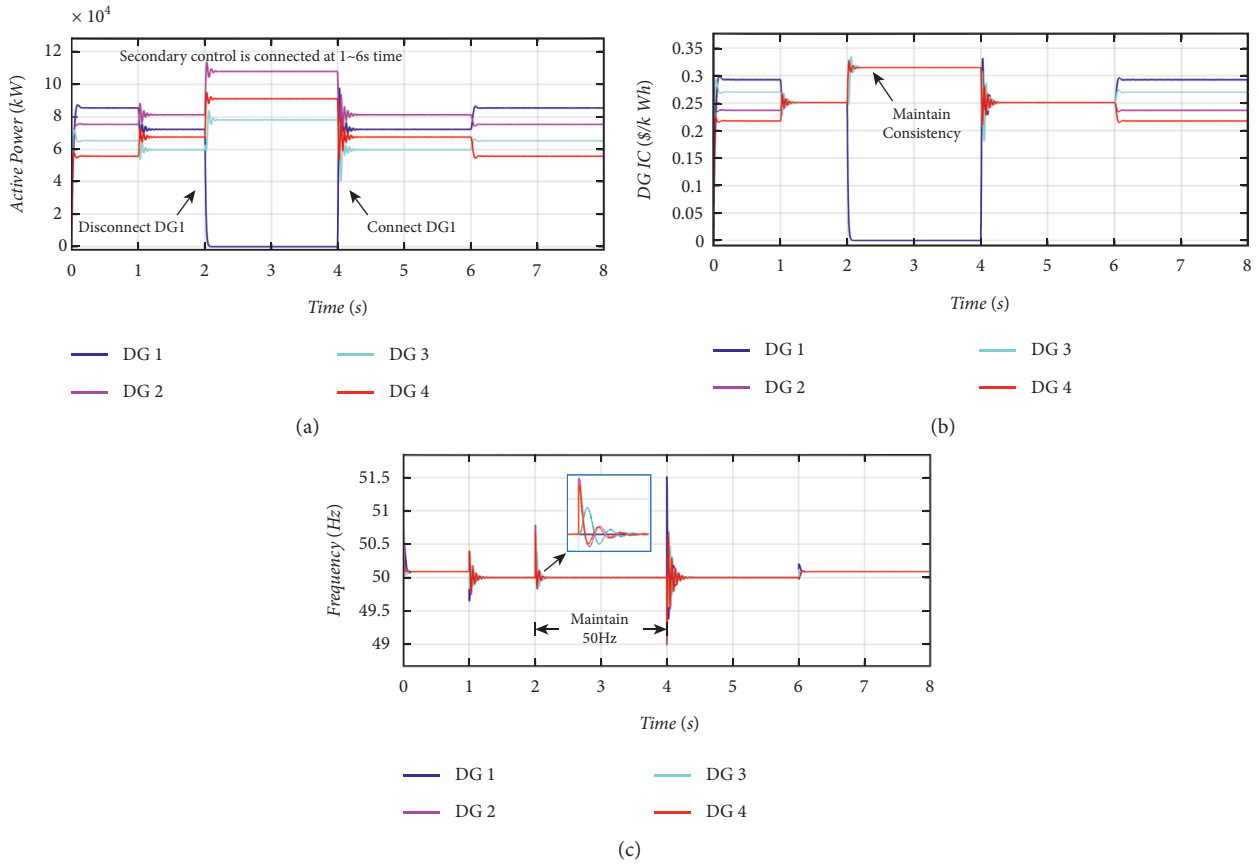

Figure 9: System plug-and-play simulation results.

As can be seen from Figures 10(a) and 10(b), when the packet loss rate is small, the impact of the attack on DG1 is mainly causes the IC curve of DG1 to produce a large overshoot during this period, which deviates from the consistent value reached by the system except for DG1. The system frequency fluctuates during the attack period and deviates from the nominal frequency of 50 Hz. As can be seen from Figures 10(c) and 10(d), when the packet loss rate is large, the consistency control of the IC in the period $t_1 \sim t_2$ fails, and the change of DG1 is the largest. The system frequency has a great overshoot at the moment of the attack and greatly deviates from the nominal frequency. Therefore it can be concluded that the main impact is the consistency control process of the IC, and the secondary control method is still effective in the rest of the time.

5.3. Verify the Effect of Improving Consistency Strategy. In order to verify the effectiveness of the improved consistency strategy based on event-triggered in the case of weaker DoS attacks for frequency restoration and power optimization of the microgrid, use the same simulation process. Select the time period $t_1 \sim t_2$ during which DoS attacks occur, and the simulation time is 2s. Assuming that at $t_1 = 1s$, the system detects DoS attacks, and then initiates the improved consistency strategy based on event-triggered. The results of changes in the IC and frequency are shown in Figure 11.

As can be seen from Figures 11(a) and 11(b), starting the improved consistency strategy can restore the destroyed IC consistency. The recovery time is about 0.05s. The system frequency can achieve stability after fluctuations. When the packet loss rate is large, as can be seen from Figures 11(c) and 11(d), the improved consistency strategy is still effective, but the consistency recovery time of the IC is prolonged, about 0.35s. The system frequency has a large overshoot during the recovery process, but it can still be stabilized at 50 Hz. It can be concluded that in the case of weaker DoS attacks, the improved consistency strategy based on event-triggered can achieve our control goals, which proves the effectiveness of the proposed strategy.

5.4. Verify the Effect of Predictive Compensation Control. As mentioned above, when an extreme situation occurs in DoS attacks, consider using the data obtained by predictive compensation control instead of the real data to complete the IC consistency control process. Select time period $t_1 \sim t_2$ when the DoS attack occurs. The changes in IC and system frequency are shown in Figure 12. When a DG suffers DoS

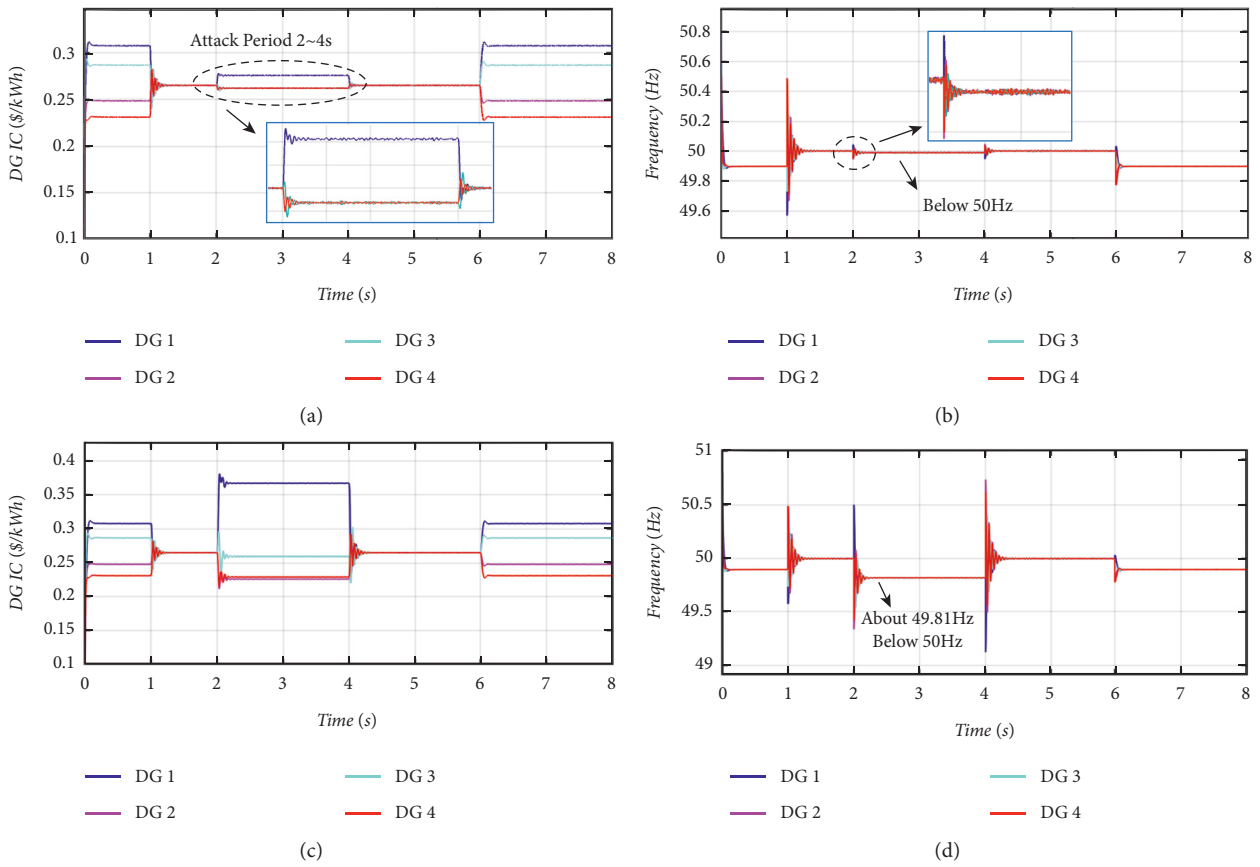

Figure 10: Comparison of the impact of DoS attacks.

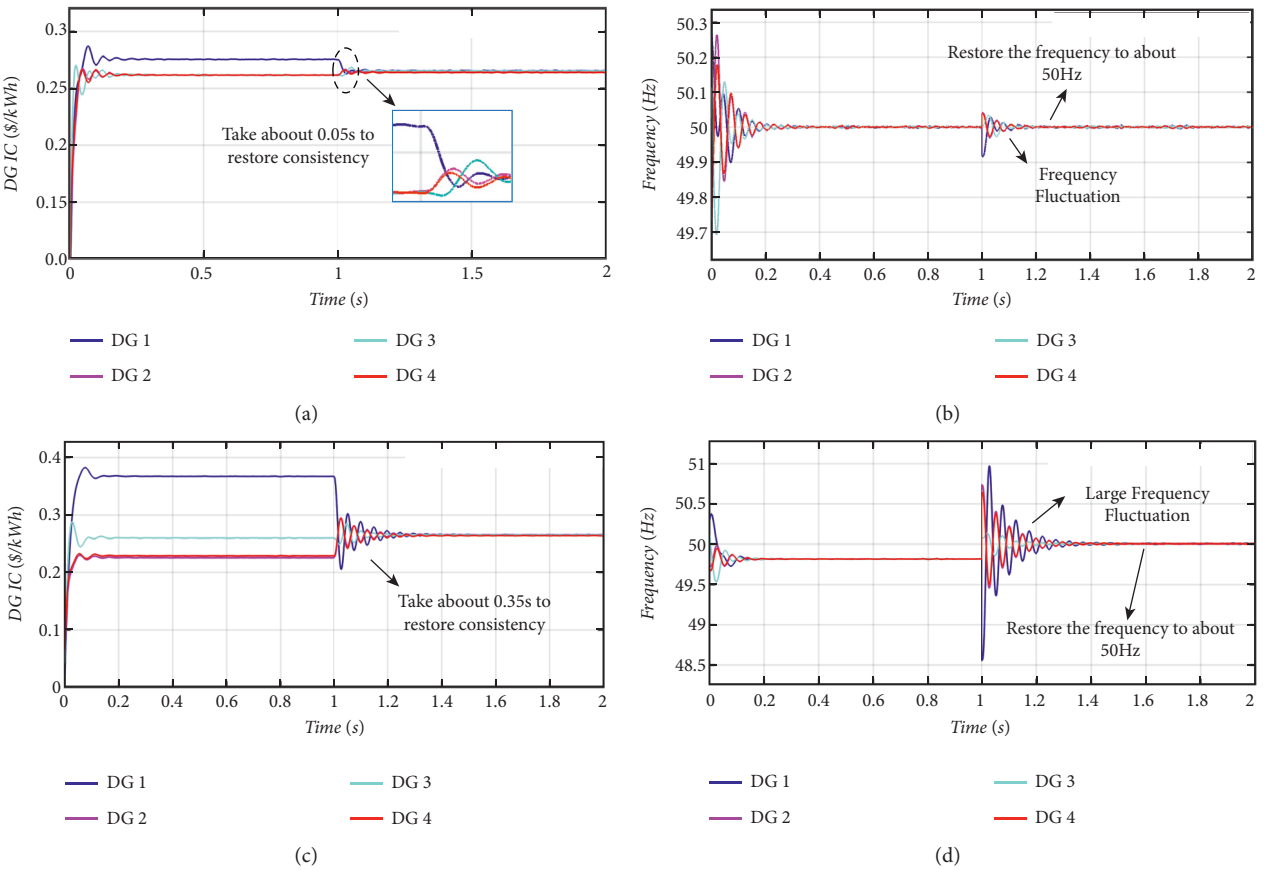

Figure 11: Comparison of control effects of improved consistency strategy.

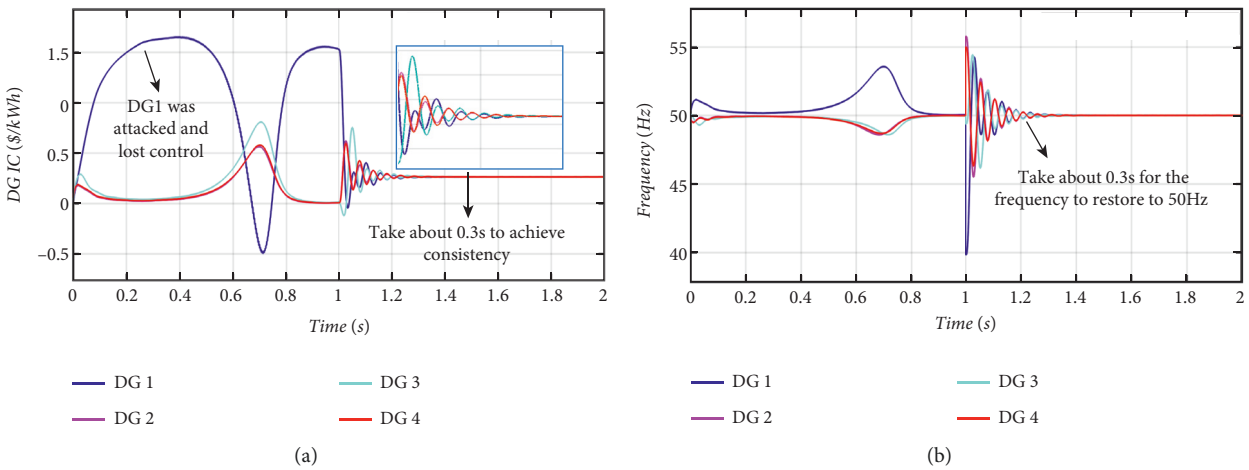

Figure 12: Predictive compensation strategy control effect diagram.

attacks to completely drop its packets, the attacks will gradually spread throughout the network, which will seriously affect the fidelity of the information. After $t_1 = 1s$, because the event-triggered mechanism calculates the impact of packet loss on the secondary control, the predicted data obtained from the output of the predictive compensation is used to replace the real data to complete the subsequent consistency control process.

As can be seen from Figures 12(a) and 12(b), the IC and frequency of each DG can be restored to be consistent at about 0.3 s. According to the above analysis, for extreme DoS attacks, the secondary control strategy based on event-triggered can well use the predictive compensation data to suppress the overshoot and complete the IC consistency control process, while stabilizing the system frequency at the nominal value.

6. Conclusion

This paper proposes a distributed two-layer control structure for the islanded microgrid system with CPS characteristics. The control structure can realize the distributed frequency adjustment and power optimization of the microgrid at the same time, effectively shortening the operating time of the system, and significantly improving the power optimization distribution capability of the microgrid. Aiming at the possible network attacks at the cyber layer, in order to reduce the impact of different degrees of DoS attacks on the system, this paper designs an improved consensus algorithm based on event-triggered and predictive compensation control that combines EMD and ELM. Finally, the 4-node MG system is simulated and analyzed, and the experimental results show that this method can effectively eliminate the influence of DoS attacks on consistency control, keep the system frequency at 50 Hz, and keep the IC consistency of all DGs. The results show that this method can meet the control requirements of frequency synchronization, frequency error-free, and optimal operation cost.

Abbreviations

CPS: Cyber-physical system
DoS: Denial-of-service
EMD: Empirical mode decomposition
ELM: Extreme learning machine
DGs: Distributed generators
MG: Microgrid
IC: Incremental cost
IMFs: Intrinsic mode functions
DGi: The i-th DGs
x_i: The state variable
u_i: The control variable
$x_{i\infty}$: The final state variable of the i-th agent
x_{i0}: The initial state variable of the i-th agent n, the total number of DGs
$a_i b_i$, c_i: The cost coefficients of DGi
l: The total number of loads
N_i: Neighbor set of agent i
$\mathbf{A}$: Adjacency matrix of the communication graph
$\mathbf{L}$: Laplacian matrix of the network
$\mathbf{E}$: The identity matrix
$\mathbf{W}(\mathbf{k}) \in \mathbf{R}^{n\times n}$: The state transition matrix of the system
C_i: The cost function of DGi
C_{total}: The total cost
P_i: The generated active power of DGi
P_{Dj}: The power of the j-th load
P_D: The power demand of the total load
$P_{i,\min}$: The minimum power generation of DGi
$P_{i,\max}$: The maximum power generation of DGi
$\lambda_i(P_i)$: The IC of DGi
f_i: The frequency emitted by DGi
Ω: The set of all DGs
f_{MG}^{ref}: The rated output frequency of the system
P_i^{ref}: The rated active power of DGi
m_i: The droop coefficient
$k_{P,i}$, $k_{I,i}$: The proportional coefficient and integral coefficient of DGi

α_i: The packet loss rate of DGi
λ_{ci}: The IC calculated by the predictive compensation control.

Data Availability

Data sharing not applicable to this article as no datasets were generated or analyzed during the current study.

Conflicts of Interest

Submission of this study does not involve any conflict of interest.

Acknowledgments

This work was supported by theNational Key R&D Program of China under grant (2018YFA0702200), Liaoning Natural Science Foundation (2021-MS-086), the National Natural Science Foundation of China (62173074), the Key Project of National Natural Science Foundation of China (U20A2019).

References

[1] V. Nikam and V. Kalkhambkar, "A review on control strategies for microgrids with distributed energy resources, energy storage systems, and electric vehicles," *International Transactions on Electrical Energy Systems*, vol. 31, no. 1, Article ID e12607, 2021.

[2] G. Shahgholian, "A brief review on microgrids: operation, applications, modeling, and control," *International Transactions on Electrical Energy Systems*, vol. 31, no. 6, Article ID e12607, 2021.

[3] B. Sahoo, S. K. Routray, and P. K. Rout, "AC, DC, and hybrid control strategies for smart microgrid application: a review," *International Transactions on Electrical Energy Systems*, vol. 31, no. 1, Article ID e12683, 2021.

[4] J. W. Simpson-Porco, Q. Shafiee, F. Dörfler, J. C. Vasquez, J. M. Guerrero, and F. Bullo, "Secondary frequency and voltage control of islanded microgrids via distributed averaging," *IEEE Transactions on Industrial Electronics*, vol. 62, no. 11, pp. 7025–7038, 2015.

[5] M. M. Mobashsher, R. Keypour, and M. Savaghebi, "Distributed optimal voltage control in islanded microgrids," *International Transactions on Electrical Energy Systems*, vol. 31, no. 11, Article ID e13045, 2021.

[6] A. Constanza and C. Boberto, "Secondary control strategies for frequency restoration in islanded microgrids with consideration of communication delays," *IEEE Transactions on Smart Grid*, vol. 7, 2016.

[7] A. Selakov, D. Bekut, and A. T. Sarić, "A novel agent-based microgrid optimal control for grid-connected, planned island and emergency island operations," *International Transactions on Electrical Energy Systems*, vol. 26, no. 9, pp. 1999–2022, 2016.

[8] F. L. Li, C. X. Dou, X. L. Hu, Z. Q. Zhang, and T. F. Zhang, "Finite-time consensus for frequency and voltage restoration in microgird under communication interruptions," *International Transactions on Electrical Energy Systems*, vol. 31, no. 4, Article ID e12830, 2021.

[9] J. B. Almada, R. P. Leão, R. G. Almeida, and R. F. Sampaio, "Microgrid distributed secondary control and energy management using multi-agent system," *International Transactions on Electrical Energy Systems*, vol. 31, no. 10, Article ID e12886, 2021.

[10] A. H. Tayebi, R. Sharifi, A. H. Salemi, and F. Faghihi, "Presentation of an H_∞ based frequency control for islanding provisional microgrid consisting of hybrid AC/DC microgrid," *International Transactions on Electrical Energy Systems*, vol. 31, no. 10, Article ID e12715, 2021.

[11] M. M. Hossain and C. Peng, "Predictive event-triggered H_∞ load frequency control for hybrid power systems under denial-of-service attacks," *IET Generation, Transmission & Distribution*, vol. 14, no. 26, pp. 6457–6467, 2020.

[12] B. Zhang, C. X. Dou, D. Yue, Z. Zhang, and T. Zhang, "A cyber-physical cooperative hierarchical control strategy for islanded microgrid facing with random communication failure," *IEEE Systems Journal*, vol. 14, no. 2, pp. 2849–2860, 2020.

[13] C. X. Huang, J. Wang, S. Deng, and D. Yue, "Real-time distributed economic dispatch scheme of grid-connected microgrid considering cyber attacks," *IET Renewable Power Generation*, vol. 14, no. 14, pp. 2750–2758, 2020.

[14] Y. J. Zhang, T. Yang, and Z. H. Tang, "Active fault-tolerant control for load frequency control in multi-area power systems with physical faults and cyberattacks," *International Transactions on Electrical Energy Systems*, vol. 31, no. 7, Article ID e12906, 2021.

[15] I. Brahmia, J. Wang, L. Oliveira, and H. Xu, "Hierarchical smart energy management strategy based on cooperative distributed economic model predictive control for multi-microgrids systems," *International Transactions on Electrical Energy Systems*, vol. 31, no. 2, Article ID e12732, 2021.

[16] Y. Y. Zou, Y. Dong, S. Y. Li, and Y. G. Niu, "Multi-time hierarchical stochastic predictive control for energy management of an island microgrid with plug-in electric vehicles," *IET Generation, Transmission & Distribution*, vol. 13, no. 10, pp. 1794–1801, 2019.

[17] H. Han, Q. P. Xia, Y. Sun, X. C. Hou, and M. Su, "Leader-distributed follower-decentralized control strategy for economic dispatch in cascaded-parallel microgrids," *International Transactions on Electrical Energy Systems*, vol. 31, no. 9, e12964, 2021.

[18] E. Shafiee Roudbari, M. T. H. Beheshti, and S. M. Rakhtala, "Voltage and frequency regulation in an islanded microgrid with PEM fuel cell based on a fuzzy logic voltage control and adaptive droop control," *IET Power Electronics*, vol. 13, no. 1, pp. 78–85, 2020.

[19] F. Dehghani, M. Tourandaz Kenari, and M. A. Shafiyi, "A novel hybrid droop control strategy for DC microgrid with simultaneous consideration of operating costs and flexibility," *International Transactions on Electrical Energy Systems*, vol. 31, no. 6, Article ID e12896, 2021.

[20] S. Rath, D. Pal, P. S. Sharma, and B. K. Panigrahi, "A cyber-secure distributed control architecture for autonomous AC microgrid," *IEEE Systems Journal*, vol. 15, no. 3, pp. 3324–3335, 2021.

[21] S. W. Zheng, K. Liao, J. W. Yang, and Z. He, "Droop-based consensus control scheme for economic dispatch in islanded microgrids," *IET Generation, Transmission & Distribution*, vol. 14, no. 20, pp. 4529–4538, 2020.

[22] H. H. Yuan, Y. Q. Xia, H. J. Yang, and Y. Yuan, "Resilient control for wireless networked control systems under DoS attack via a hierarchical game," *International Journal of Robust and Nonlinear Control*, vol. 28, no. 15, pp. 4604–4623, 2018.

[23] B. Y. Wang, Q. Y. Sun, R. K. Han, and D. Ma, "Consensus-based secondary frequency control under denial-of-service attacks of distributed generations for microgrids," *Journal of the Franklin Institute*, vol. 358, no. 1, pp. 114–130, 2021.

[24] B. J. Karaki and M. S. Mahmoud, "Scaled consensus design for multiagent systems under DoS attacks and communication-delays," *Journal of the Franklin Institute*, vol. 358, no. 7, pp. 3901–3918, 2021.

[25] Y. Li, F. Y. Song, J. L. Liu, X. Xie, and E. Tian, "Decentralized event-triggered synchronization control for complex networks with nonperiodic DoS attacks," *International Journal of Robust and Nonlinear Control*, vol. 32, no. 3, pp. 1–21, 2021.

[26] Y. C. Sun and G. H. Yang, "Robust event-triggered model predictive control for cyber-physical systems under denial-of-service attacks," *International Journal of Robust and Nonlinear Control*, vol. 29, no. 14, pp. 4797–4811, 2019.

[27] W. Wenjun, T. Binfeng, H. Julong, and G. Fengyang, "Hierarchical optimization strategy for microgrid based on finite-time consensus algorithm," *Proceedings of the CSU-EPSA*, vol. 32, no. 6, pp. 7–13, 2020.